Thermal Resolution of Unblocking Temperatures (TROUT): A method for "unmixing" multi-component magnetizations

Brendan Cych[1], Matthias Morzfeld[1], David Heslop[2], Sarah Maher[1], Jeffrey Gee[1], Lisa Tauxe[1]

[1]Scripps Institution of Oceanography, University of California, San Diego, CA, USA
[2]Research School of Earth Sciences, Australian National University, Canberra, ACT, Australia

Key Points:

- Multi-component thermal demagnetization experiments can exhibit curved demagnetization data, causing ambiguity in estimating the temperature the specimen was reheated to.
- TROUT is a method for resolving the unblocking temperature distributions, directions and relative magnitudes of different components present in demagnetization data.
- TROUT accurately estimates the temperature specimens were reheated to in laboratory experiments, even for those with curved demagnetization data.

Corresponding author: Brendan Cych, bcych@ucsd.edu

Abstract

Some rocks contain multiple remanence "components", each of which preserves a record of a different magnetic field. The temperature ranges over which these remanence components demagnetize can overlap, making it difficult to determine their directions. We present a data analysis tool called Thermal Resolution Of Unblocking Temperatures (TROUT) that treats the process of thermal demagnetization as a function of temperature (or alternating field demagnetization as a function of coercivity). TROUT models the unblocking temperature distributions of components in a demagnetization experiment, allowing these distributions to overlap. TROUT can be used to find the temperatures over which paleomagnetic directions change and when two directional components overlap resulting in curved demagnetization trajectories. When applied to specimens given multicomponent Thermoremanent Magnetizations (TRMs) in the laboratory, the TROUT method estimates the temperature at which the partial TRMs were acquired to within one temperature step, even for specimens with significant overlap. TROUT has numerous applications: knowing the temperature at which the direction changes is useful for experiments in which the thermal history of a specimen is of interest (e.g. emplacement temperature of pyroclastic deposits, re-heating of archaeological artifacts, reconstruction of cooling rates of igneous bodies). The ability to determine whether a single component or multiple components are demagnetizing at a given temperature is useful for choosing appropriate ranges of temperatures to use in paleointensity experiments. Finally, the width of the range of temperature overlap may be useful for inferring the domain state of magnetic mineral assemblages.

Plain Language Summary

Rocks can contain records of multiple magnetization events or "components". Paleomagnetists attempt to separate these components by heating their specimens to progressively higher temperatures, and cooling in the absence of a magnetic field to remove part of the magnetization. Paleomagnetists are often interested in the temperature range over which one of the magnetization components is demagnetized, as this provides information about the thermal history of the specimen (e.g. the temperature it was reheated to in the past). Unfortunately, two components can demagnetize with overlapping temperature ranges, leading to ambiguity in the temperatures of interest. In this paper we present a data analysis tool called Thermal Resolution of Unblocking Temperatures (TROUT) which can account for this overlap and find the temperatures that paleomagnetists are interested in. We tested TROUT on data sets where the temperatures the specimens were reheated to is known, and it accurately estimated those temperatures. These test cases indicate that TROUT will be useful for many different applications where paleomagnetists want to know about the thermal history of a specimen.

1 Introduction

Paleomagnetists use the magnetizations of rocks to make inferences about the Earth's ancient magnetic field (Butler, 1992). A rock that cools in a magnetic field obtains a magnetization in the same direction as that field. In theory, a paleomagnetist could take an oriented paleomagnetic specimen and measure its magnetization to obtain the direction of the ancient magnetic field. Unfortunately, many rocks have experienced multiple magnetization events in different field directions, causing them to have a total magnetization which is the sum of multiple magnetic "components" acquired in these different fields. To separate out the individual components, paleomagnetists demagnetize specimens in a stepwise fashion by heating them at progressively higher temperatures and cooling them in the absence of a magnetic field to demagnetize them (Worm et al., 1988). Strong alternating magnetic fields may also be used to demagnetize a specimen. Experiments like

these that involve some form of stepwise demagnetization are ubiquitous in paleomagnetic studies.

Data from a thermal or alternating field (AF) demagnetization experiments are typically plotted on the Zijderveld diagram (Zijderveld, 1967), whereby the X coordinate of the direction is plotted against the Y and Z coordinates (Figure 1) allowing visualization of inherently three dimensional behavior on a two-dimensional plot (X,Y and Z are equivalent to North, East and Down in oriented specimens). Data with a single magnetic component will plot as a pair of straight lines trending toward the origin. For a two-component magnetization, as the specimen is demagnetized the data will plot as straight lines which do not trend toward the origin at low temperatures (fields). At higher temperatures (fields), the direction of the lines will change, with a trend toward the origin. The directions of these lines are parallel to the direction of the two fields in which the specimen was magnetized. An example of this two component behavior for a simulated thermal demagnetization expriment is shown in Figure 1a. In some cases, instead of distinct lines with sharp boundaries (as in Figure 1a), the change in direction appears to happen over several temperature steps, leading to a "curved" appearance in the Zijderveld plot (Figure 1b). This behavior makes multi-component magnetizations more difficult to interpret, as the demagnetization experiment has failed to completely separate the two components.

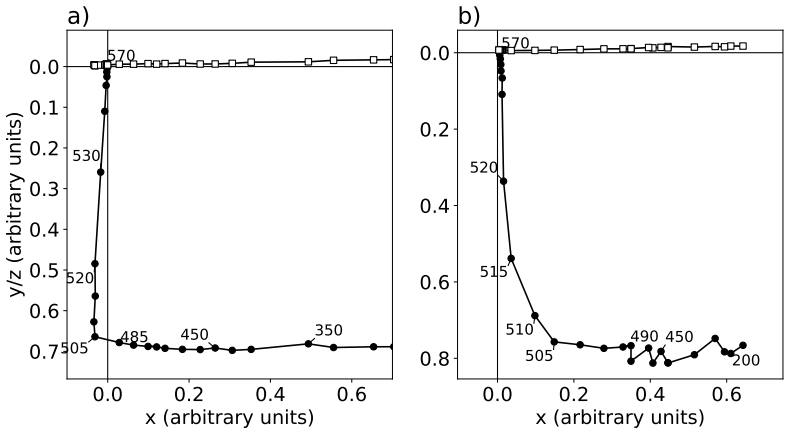

Figure 1: Examples of Zijderveld plots. Solid (open) symbols: x versus y (z). a) A specimen with two relatively straight, resolvable magnetization components in perpendicular directions. b) Another specimen, magnetized in the same way as in a), but displaying two components with overlapping unblocking temperatures. The resulting Zijderveld plot has a "curved" appearance.

Demagnetization experiments are able to separate multiple magnetic components because rocks are composed of many nano- to micrometer scale magnetic particles. Louis Néel proposed a theory (Néel, 1949) that these magnetic particles can be magnetized in one of two directions, and some amount of energy is required to 'flip' their magnetic moment from one 'easy' direction to the other. While this is not generally true (e.g., Nagy et al., 2022), the concept of thermal energy and remagnetization holds true. Partial demagnetization of a specimen is achieved by randomizing the moments of particles with energy barriers that can be overcome by the thermal or AF treatment step. In a thermal demagnetization experiment, this occurs at a particular temperature, known as the "unblocking temperature" (T_{ub}). In AF demagnetization, the field provides the energy to flip the moment of the particle. Néel theory suggests that a magnetic component acquired by heating to a particular temperature, the blocking temperature (T_b), and cool-

ing in a field would be removed by thermally demagnetizing that specimen to the same temperature $T_b = T_{ub}$. However, Néel theory applies only to uniformly magnetized or "single domain" magnetic particles. Micromagnetic modeling has shown that only small particles are magnetized in this way. Larger particles have more complex magnetizations such as 'flower', 'vortex' or multi-domain states (Williams & Dunlop, 1989), which may have differences between the temperature at which particles block and unblock (Dunlop & Özdemir, 2001). This can lead to an "overlap" of the unblocking temperatures between components blocked at different temperatures resulting in the curvature observed on the Zijderveld plot in Figure 1b. Overlapping of the unblocking temperatures may also occur if two components are not magnetized in the same way, e.g. a specimen containing both a thermally acquired and a chemically acquired remanence. Additionally, specimens which moved during cooling, or which cooled slowly as the direction of the Earth's magnetic field changed, may have curved Zijderveld plots due to the rotation of the specimen relative to the field.

Previous studies have dealt with isolating individual directions from multi-component magnetizations with overlapping unblocking temperatures. Hoffman and Day (1978) created a generalized method for separating overlapping multi-component directions by fitting great circle paths to the vector differences of demagnetization data. Kirschvink (1980) created a method for obtaining best fitting lines or planes to paleomagnetic data using principal component analysis, and McFadden and McElhinny (1988) extended this methodology to find a common paleomagnetic direction using the intersection of lines and planes from different paleomagnetic specimens. None of these methods quantitatively provide information about the unblocking temperature ranges over which different components demagnetize when the unblocking temperatures overlap. However, this information is important in several applications, for example, when performing paleodirectional/intensity analysis. In such a case, paleomagnetists attempt to choose a range of temperatures on the Zijderveld plot over which a single remanence component unblocks. The blocking temperature distribution of each component is also useful for determining the temperature at which a pyroclastic flow came to rest (also known as the emplacement temperature), or to find the temperature to which a host rock was reheated by an intruding igneous dike (a form of "baked contact test", as per Everitt & Clegg, 1962).

In this paper, we present a method for treating demagnetization data which can obtain the direction, relative magnitude, and unblocking temperature (or coercivity) distribution for each component in a demagnetization experiment. If the unblocking temperature (coercivity) distributions are separate, then the components will be easily resolvable (Figure 2a, c). If the distributions overlap with one another, then the components will be hard to resolve (Figure 2b,d). We call our approach "Thermal Resolution of Unblocking Temperatures" (TROUT). The construction of this model is explained in Section 2 and we explain how to fit the model to real demagnetization data in Section 2.2.

One advantage that TROUT has over traditional methods of analyzing demagnetization data is the ability to obtain information about the range of unblocking temperatures for a particular component. For example, TROUT can obtain an estimate of the temperature to which a specimen was remagnetized, as well as the range of temperatures over which two components overlap (see Section 2.4). In Section 3 the TROUT method is applied to several data sets that make use of this thermal information. In Section 3.1 we extend the work of Maher et al. (2021) to test whether their specimens have reproducible unblocking temperatures that could be used to estimate a quantitative cooling rate for fast spreading lower oceanic crust. In Section 3.2, we remagnetized specimens from Tauxe et al. (2021) to test TROUT's ability to obtain the remagnetization temperatures and directions for a set of specimens which may have different blocking and unblocking temperature distributions. In Section 3.3, we replicate the experimental results of Kent and Gee (1994) in which specimens were given a secondary magnetization at low temperatures to test whether high blocking temperatures observed in previous

thermal demagnetization experiments were a result of specimens undergoing chemical alteration during heating. We discuss our findings in Section 4.

2 Methodology

2.1 Modeling magnetization as a function of demagnetizing energy

The goal of this work is to model thermal demagnetization in a specimen with multiple components. We start with the simpler, uni-vectorial case. A specimen with a single magnetic component will have a magnetization which reduces in magnitude but maintains a constant direction as it is demagnetized. Here, the energy used to demagnetize the specimen is called x and it is possible to obtain an expression for the magnetization remaining as a function of x, $\vec{M}(x)$. The field direction is represented by the symbol $\hat{B}$ (a unit vector) and the original magnitude of the magnetization before demagnetizing is represented by c. An expression is required for the amount of the magnetization that survives after demagnetizing to x. The resulting "demagnetization function" $F(x)$ should vary between 1 at $x = 0$ and 0 at some maximum value for x. The full equation of the magnetization is the product of these three terms:

$$\vec{M}(x) = c\hat{B}F(x). \tag{1}$$

In the more complicated multi-component case, a specimen may record multiple (re)magnetization events, and so may have multiple (K) components. In this case, the magnetization is the sum of the magnetizations of the components, i.e.

$$\vec{M}(x) = \sum_{k=1}^{K} c_k \hat{B}_k F_k(x). \tag{2}$$

There is no requirement that any two demagnetization functions F_i and F_j operate over independent temperature ranges, and so this model can be used to simulate specimens with overlapping unblocking temperatures, provided there is some expression for F.

The way to represent the problem of mixed TRM components is very similar to the problem of unmixing Isothermal Remanent Magnetization (IRM) components (e.g., Egli, 2003). These experiments use an alternating field to demagnetize a magnetization acquired in a strong magnetic field at room temperature. The magnitude of the magnetization at each demagnetization step is used to infer several "components" which have different coercivity distributions. In the IRM unmixing literature, a "component" usually refers to a subpopulation of magnetic particles interpreted as representing a particular magnetic mineral, whereas in TRM unmixing, a component refers to a set of particles magnetized in a particular magnetic field direction. Both types of components require a flexible function to model the wide range of demagnetization curves observed in natural samples.

For the purposes of IRM unmixing, Egli (2003) created a four parameter Skew Generalized Gaussian (SGG) Distribution given by:

$$f(x, \mu, s, p, q) = \frac{1}{2^{1+1/p} s \Gamma(1 + 1/p)} \frac{|qe^{qz} + q^{-1}e^{z/q}|}{e^{qz} + e^{z/q}} \exp\left[-\frac{1}{2} \left| \ln\left(\frac{e^{qz} + e^{z/q}}{2} \right) \right|^p \right], \tag{3}$$

where $z = \frac{x-\mu}{s}$ and Γ is the gamma function; the scalar parameters μ, s, p, q determine the "shape" of the distribution. To first order, μ controls the location of the distribution, s controls the scale, p controls the kurtosis and q controls the skewness, although interactions between these parameters mean that they do not independently affect these properties of the distribution. SGG distributions are able to approximate a wide range of other distributions by selecting μ, s, p, q appropriately. For this reason, SGGs are useful for our purposes. In the work of Egli (2003), the SGG distribution is scaled and fit

to the negative derivative of the magnitude of the demagnetization data with respect to x. In the case of IRMs, this quantity represents the coercivity distribution, and in the TRM case, the unblocking temperature distribution of the magnetization. The demagnetization function is therefore given by:

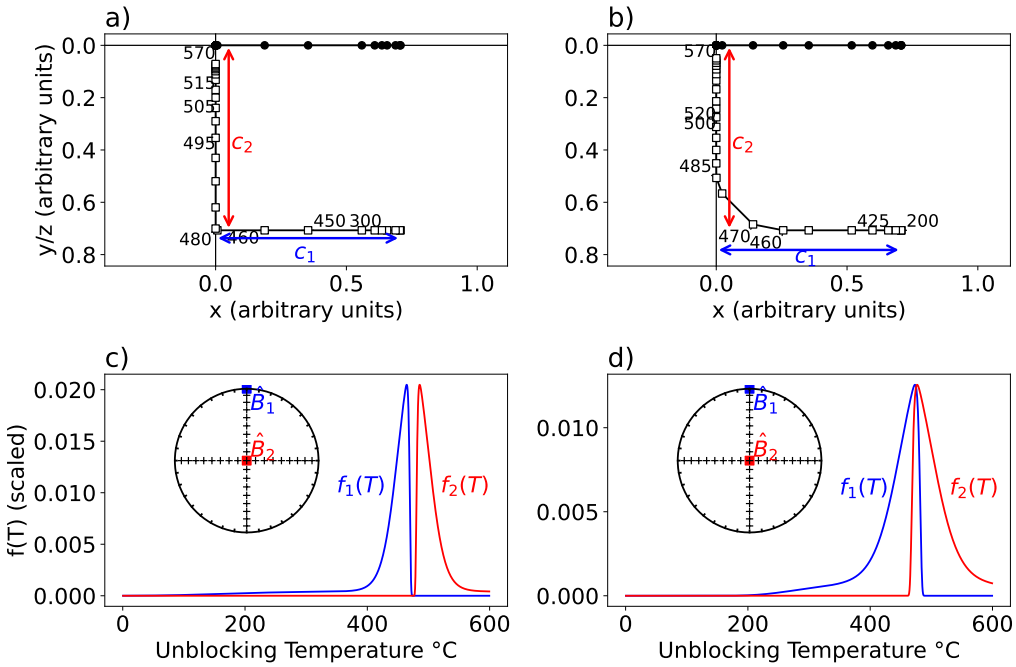

Figure 2: Simulated two-component thermal demagnetization data subjected to TROUT. For more information on the different parameters referenced in this figure, see Section 2. Panels a) and b): Simulated Zijderveld plots with the magnitude of each component (c_k) indicated by blue and red arrows. Solid (open) symbols are X,Y (X,Z) components. Panels c) and d): unblocking temperature density functions $f(T, \mu_k, s_k, p_k, q_k)$ for each component obtained from the TROUT method. Left column: Example without overlapping unblocking temperatures. Right column: Example with overlapping unblocking temperatures. High (low) temperature components indicated in red (blue). In d) the unblocking temperature density clearly displays overlap between the unblocking temperature functions. Insets: Equal area plots of the directions $\hat{B}_k$ of each component. Center of diagram is the Z (vertical) direction, top (right) edge is the X (Y) direction. B_1 (B_2) was acquired along the X (Z) specimen direction.

$$F(x, \mu, s, p, q) = 1 - \int f(x, \mu, s, p, q)\, dx. \tag{4}$$

Figure 2 shows simulated thermal demagnetization experiments for the case of non-overlapping unblocking temperatures (Figure 2a, c) and the case of overlapping unblocking temperatures (Figure 2b, d). The following sections explain how the TROUT approach is used to find the unblocking temperature distributions and directions that provide the best fit to thermal demagnetization data, allowing quantification of the temperature that separates the two components and the amount of overlap in unblocking temperatures between two components.

2.2 Fitting TROUT to data

The TROUT model in Equation 2 describes magnetization as a function of temperature. The model includes several "model parameters" that define the unblocking temperature distributions, directions and relative magnitudes of each component. A framework is needed for fitting the TROUT model to the data by selecting model parameters that lead to model outputs that are comparable to the data. Model fitting is performed via optimization of a Bayesian posterior distribution, which synthesizes prior information about the parameters with model-data misfit (see, e.g., Tarantola, 2005). Specifically, the posterior distribution is proportional to the product of a likelihood that describes the model-data misfit, and a prior distribution that specifies additional information about the model parameters. By finding the maximum value of the posterior distribution, TROUT thus finds the model that best fits the data, while simultaneously satisfying prior constraints and, therefore, avoids overfitting. The following describes how to set up the likelihood and prior distributions and how to solve the resulting optimization problem.

2.2.1 Likelihood

We begin with the likelihood that specifies how model-data misfit is quantified. The unknowns of the TROUT model in Equation 2 are $c, \hat{B}$ and the function $F(x)$, which is parameterized via Equations 3 and 4, adding the unknowns μ, s, p and q. To simplify notation, all unknowns are collected in a vector $\theta = (c, \hat{B}, \mu, s, p, q)$. Then the model data misfit is defined by the quadratic:

$$\text{Misfit} = \frac{1}{2}(\vec{M}(x,\theta)_{pred} - \vec{M}_{obs})^T C^{-1} (\vec{M}(x,\theta)_{pred} - \vec{M}_{obs}), \tag{5}$$

where $\vec{M}_{pred}(x)$ is given by Equation 2, $\vec{M}_{obs}(x)$ is the observed magnetization, and C is a matrix that describes errors in the data. The misfit and likelihood are connected via an exponential

$$p(M_{obs}|\theta) = (\det 2\pi C)^{-\frac{1}{2}} \exp\left(-\frac{1}{2}(\vec{M}(x,\theta)_{pred} - \vec{M}_{obs})^T C^{-1} (\vec{M}(x,\theta)_{pred} - \vec{M}_{obs})\right). \tag{6}$$

To specify the error covariance matrix C, it is important to recall that when paleomagnetic measurements are made, a significant proportion of measurement error comes from misorientation of specimens in the sample holder, which results in an angular misfit (see for example Paterson et al., 2012 for a discussion). This should be correctly reflected by the choice of C in the likelihood. Holme and Bloxham (1996) devised an error matrix for satellite data, where there are similarly two kinds of noise, measurement errors as well as "attitude errors," caused by misorientation and this can be adapted to the problem at hand. Specifically, we use the error covariance matrix:

$$C = I(\sigma^2 + |\vec{M}|^2\psi^2) - \vec{M}\vec{M}^T\psi^2, \tag{7}$$

where ψ (an angle in radians) and σ (a constant measurement uncertainty for all data) are unknown parameters that define the noise distribution. Note that the the unknown parameters in the error covariance matrix can be estimated by simply appending them to the model parameter vector $\theta = (c, \hat{B}, \mu, s, p, q, \sigma, \psi)$ and subsequently defining the posterior jointly over all unknowns (see below). Finally, for a set of N measurements, the likelihood is the product of the likelihoods for each measurement:

$$P(\vec{M}_{obs}|\theta) = \prod_{i=1}^{N} P(\vec{M}_{obs}(x_i)|\theta). \tag{8}$$

It is worth re-emphasizing that θ includes the unknown parameters defining the measurement noise. Two examples of this noise model and the resulting likelihoods are shown in Figure 3.

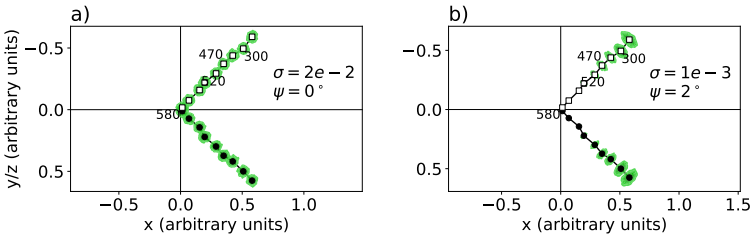

Figure 3: Examples of the likelihood distribution (green shaded areas) for an idealized single component Arai plot (Zijderveld data). The TROUT method prioritizes solutions which have maximum likelihood, i.e., are closest to the center of each green area for each data point. a) shows the likelihood distribution with constant noise $\sigma = 2e-2$, $\psi = 0°$, whereas b) shows the likelihood distribution with predominantly angular noise $\sigma = 1e-3$, $\psi = 2°$. In b) the angular noise causes the likelihood distribution to become spread out in a plane perpendicular to the direction of the Zijderveld data.

Table 1: Lower and upper bounds used in calculating the prior distributions of TROUT model parameters.

Parameter	c	μ	s	p^*	q^*	ψ	σ
Lower bound	0	$x_{\min}$	0	0	-5	0	0
Upper bound	$2\max(\lvert\vec{(M)}_{obs}\rvert)$	$x_{\max}$	$\frac{10}{6}(x_{\max} - x_{\min})$	5	5	$\frac{\pi}{18}$	∞

2.2.2 Prior Distribution

A prior distribution incorporates all the information that may exist about parameters before any data are collected. Priors impose constraints on the model parameters and ameliorate issues of non-uniqueness by focusing on solutions that are in line with any of this additional information. We now describe how the prior in TROUT is constructed.

First, upper and lower bounds are imposed on all parameters, which are listed in Table 1. Here, re-scaled variables p^* and q^* are used, defined as:

$$q^* = \cot(\frac{\pi}{2}q), \quad p^* = \ln(p). \tag{9}$$

q is rescaled because SGG distributions with q values of both 1 and -1 have zero skewness, and the skewness of the distribution tends towards infinity or negative infinity as q tends towards zero from either side. For the rescaled variable, $q^* = 0$ corresponds to an SGG with zero skewness, and $|q^*| \to \infty$ implies that the skewness tends to infinity, with the direction being determined by the sign of q^*. The log-transformation on p is for convenience.

For the noise parameter σ, an "improper prior" $P(\sigma) \propto 1/\sigma$ is used, which is a popular choice and equivalent to a uniform prior over $\log\sigma$, hence easily enforcing the constraint that $\sigma > 0$. For the parameter ψ a uniform prior $P(\psi)$ is imposed, which means that all values between the lower and upper bounds have equal probability. The parameter $\hat{B}$ is a unit vector and its prior distribution is uniform on the unit sphere. Moreover, σ, $\hat{B}$ and ψ are independent of each other and of all other parameters.

For the model parameters c, μ, s, p, q we define a more complex prior that promotes non-overlapping distributions. The reason is that if two models fit the data equally well, it would be expected that the one with the smallest overlap between unblocking temperatures would be the correct one (in the majority of cases, see also below). A prior that yields the least overlapping solution that fits the data well is desired.

To quantify "overlap" between two distributions, TROUT uses a modified version of the non-parametric overlap coefficient of Inman and Bradley (1989). For any two distributions, this coefficient is given by:

$$\eta(i,j) = \int_{-\infty}^{\infty} \min\left[f_i(x), f_j(x)\right] dx. \tag{10}$$

The TROUT modification accounts for the scaling of the distributions:

$$\eta(i,j) = \frac{1}{\min(c_i, c_j)} \int_{-\infty}^{\infty} \min\left[c_i f_i(x), c_j f_j(x)\right] dx. \tag{11}$$

The coefficient $\eta(i,j)$ gives a value between 0 (no overlap between f_i and f_j) and 1 (total overlap, one distribution entirely contained within the other). Examples of the overlap coefficient for pairs of distributions are given in Figure 4. To penalize pairs of distributions with strongly overlapping unblocking temperatures in the model, the informative prior distribution $P(\eta) \sim \text{Beta}(1, 10)$ is used. For specimens with more than two components, η is computed for every pair of components. Since η is a function of the parameters c, μ, s, p, q (via f in Equation 3), $P(\eta)$ defines the prior distribution on c, μ, s, p, q, and it is worth noting that c, μ, s, p, q are not independent of each other, but they are independent of σ, $\hat{B}$ and ψ. The prior over all parameters is thus

$$P(c, \hat{B}, \mu, s, p^*, q^*, \psi, \sigma) = P(\sigma)P(\hat{B}, \psi)P(c, \mu, s, p^*, q^*) \tag{12}$$

Finally, in some cases, (e.g., when two components that are not TRMs are thermally demagnetized), a model with more overlap may be correct, which is in contradiction to the prior. In this case, however, information about the unblocking temperature distributions may not be particularly helpful, and other methods such as the plane fitting method of McFadden and McElhinny (1988) exist for obtaining directions. For this reason, promoting little overlap by construction of the prior is justified in the majority of cases considered here.

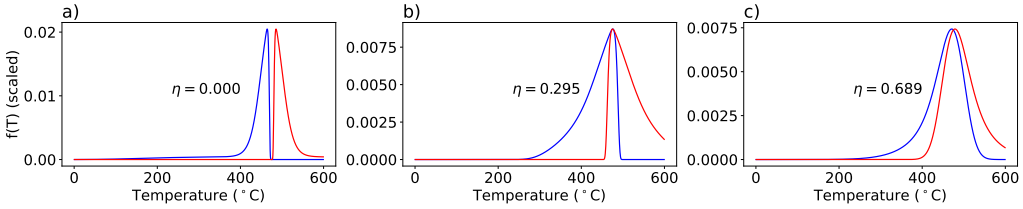

Figure 4: Examples of the overlap coefficient (η) for three different pairs of SGG distributions. In a), there is no overlap between the two distributions, so $\eta = 0$. In b) there is a significant overlap between the two distributions, so $\eta = 0.295$. In c) the two distributions are highly overlapping, so $\eta = 0.689$

2.2.3 Estimating the maximum of the posterior distribution

The posterior distribution is the product of likelihood and prior, specifically,

$$P(\theta|\vec{M}_{obs}) = P(\vec{M}_{obs}|\theta)P(\theta), \tag{13}$$

where the likelihood $P(\vec{M}_{obs}|\theta)$ is as in Equation 6 and $P(\theta)$ is shorthand notation for the prior distribution (recall that $\theta = (c, \hat{B}, \mu, s, p^*, q^*, \sigma, \psi)$). The prior can be broken down into separate parts as in Equation 12 where $P(\hat{B}, \psi)$ is a uniform prior, $P(\sigma)$ is the improper prior, and where $P(c, \mu, s, p^*, q^*)$ enforces the non-overlap condition via a prior in η in Equation 11.

To obtain unblocking temperature distributions, directions and magnitudes of each of the components, the set of model parameters with maximum posterior probability is found. First, an informed guess for the maximum posterior solution is computed, assuming that there is no overlap between the components. Details of how this best guess is computed are given in Appendix A. To obtain the set of model parameters that maximizes the posterior, the Broyden-Fletcher-Goldfarb-Shanno (BFGS, Nocedal & Wright, 2006, pp. 136) method of optimization is used. This algorithm uses the gradient of the posterior distribution (computed via finite differencing) to find a local maximum. Because the BFGS algorithm is designed to find a local maximum for a posterior distribution, and the posterior distribution may have multiple maxima, the BFGS algorithm is run multiple times on randomly generated sets of model parameters close to the best guess. A similar scheme is used by Zhao et al. (2018) to initialize optimizations for IRM unmixing. The BFGS method is deemed to have found a "maximum" when the gradient of the function reaches some minimum threshold, which may not necessarily be zero. To improve on the results of the BFGS optimization, the optimization result with the largest posterior value is picked from the outcomes of all random initializations. After this, a second optimization is run using the gradient free algorithm of Nelder and Mead (1965) to get even closer to the (global) maximum of the posterior distribution than the gradient-based BFGS method.

2.3 Rescaling of data

To be able to more easily fit SGG distributions to IRM data, Egli (2003) scaled coercivities x by a power β; $x' = x^\beta$. This is done because coercivity distributions may often be highly skewed toward values near $x = 0$, but may not be well approximated by a log distribution. Egli performed this scaling such that the IRM as a function of x' "has symmetry closest to a hyperbolic tangent distribution".

In the TROUT method, a similar scaling of data is employed to fit SGG distributions better. In contrast to coercivity distributions, unblocking temperatures may be highly skewed such that most of the unblocking occurs close to the Curie temperature. To account for the family of possible cases, the thermally unblocked data are scaled by a constant, γ, to produce a scaled version of the demagnetization energy $x'(x, \gamma)$:

$$x' = \begin{cases} x^{\exp(-|\gamma|)} & \gamma < 0 \\ x & \gamma = 0 \\ \mathbf{max}[(x_{max} - x)^{\exp(-|\gamma|)}] - (x_{max} - x)^{\exp(-|\gamma|)} & \gamma > 0. \end{cases} \tag{14}$$

As in Egli, 2003, the value of γ is chosen by minimizing the fit to a hyperbolic tangent function. For TROUT, this is done by minimizing:

$$[\mathrm{VDS}(x') - (1 - \tanh(\alpha x'/x'_{max} - \alpha/2))/2]^2, \tag{15}$$

where $\mathrm{VDS}(x')$ is the vector difference sum (Tauxe & Staudigel, 2004) of all $M(x \geq x')$. Here, α is a free parameter that controls the width of the hyperbolic tangent function. (see Figure 5 for an example). In this case, the SGG distributions are fit to the scaled data, to obtain a function $F'(x')$. This can then be converted back to $F(x)$ using a change of parameters.

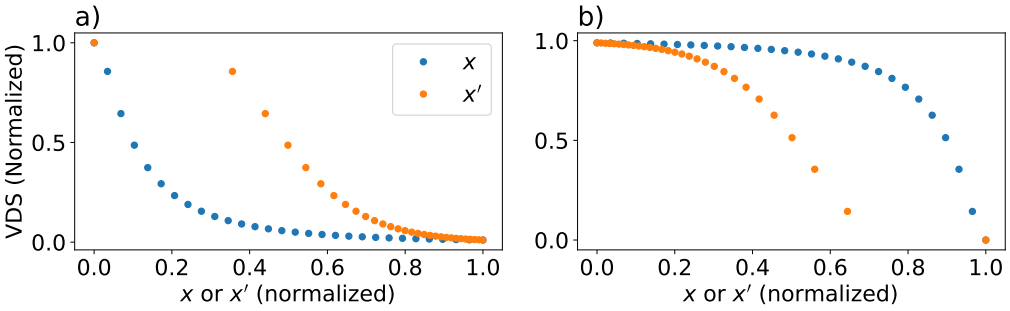

Figure 5: Examples of rescaling data from x (blue) to x' (orange) when a) $\gamma < 0$ and b) $\gamma > 0$. The rescaling improves the fitting of distributions to the data by increasing the spacing between points where the magnetization varies strongly and reducing spacing between points where the magnetization does not vary.

2.4 Interpreting results from the TROUT model

From the TROUT model defined here, two pieces of information are desired. Firstly, an estimate of the temperature a specimen was reheated to or the temperature the specimen reached as the field changed. Secondly, the range of temperatures where only one component is unblocking, e.g. for use in a paleointensity experiments where it is important to retrieve a single field strength. To assess which components are unblocking at a given temperature, we define a parameter π for each component. For the k_{th} component, π_k is the ratio of the unblocking temperature distribution to the sum of all the unblocking temperature distributions, or: $\pi_k(x) = \frac{c_k f_k(x)}{\sum_{k=1}^{K} c_k f_k(x)}$. Thus for the k_{th} component, $\pi_k \approx 1$ when that component is unblocking. If $\pi_k \approx 0$ then a different component is unblocking. If more than one component is unblocking at the same time, then $0 < \pi_k < 1$.

For any two components, there is a "Crossover Temperature" (CT) at which $\pi_i = \pi_j$, which represents the temperature to which a specimen was reheated (if the blocking and unblocking temperatures are equal). In addition to CT, there is a "mixed region" (MR), which is defined as the area where $\max[\pi_i, \pi_j] < 0.95$ and $f_i, f_j > 0$.

Outside the mixed regions, a single component is unblocking. If there is no overlap between two components, then the crossover temperature is defined slightly differently. First, temperature ranges are found where $f_i, f_j > 0$ and $\max[\pi_i, \pi_j] > 0.5$. The MR is then defined as being the range of temperatures between those two points and the CT as being the center point of this range. Conversely, some distributions may have two crossover temperatures as they intersect twice. If a single crossover temperature is required, the one with the highest $f_i = f_j$ is selected. Examples of the crossover temperature and mixed region in different cases are shown in Figure 6.

3 Applications

We now illustrate TROUT by applying it to three data sets and discuss the TROUT procedure and results in detail. The first data set is from a set of specimens from the Pito Deep in the Pacific Ocean, which were remagnetized in the laboratory by Maher et al. (2021). The second data set is from specimens exhibiting 'fragile curvature' described by Tauxe et al. (2021). And the third data set is from Mid-Ocean Ridge Basalt (MORB) specimens initially described by Kent and Gee (1994).

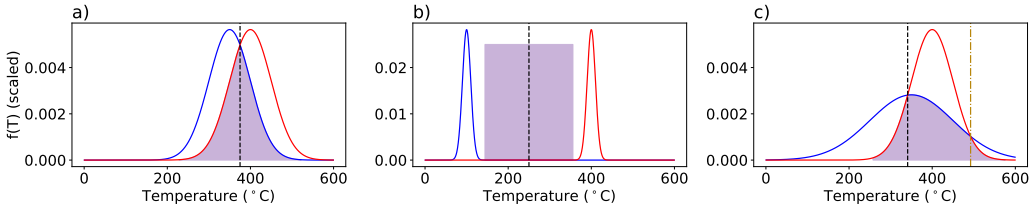

Figure 6: Illustration of the "crossover temperature" (vertical line) and "mixed region" (MR, purple shaded region) for three pairs of unblocking temperature distributions. a) Shows the simplest case, in which the two distributions overlap. b) Shows another common case, in which the two distributions do not overlap, and the MR is interpreted as being in between the two distributions, and the crossover temperature is in the center of the MR. c) Shows a rare case, in which both distributions overlap in such a way that there are two crossover temperatures. The crossover temperature at which the unblocking temperature distributions are largest is preferred in this case.

3.1 Pito Deep Specimens

Maher et al. (2021) documented numerous examples of samples with multicomponent remanences from tectonic exposures of the lower oceanic crust at Pito Deep (∼23°S, 112°W). These multicomponent remanences provide information about the thermal history of the lower crust, as they imply that the rocks cooled over a long time during which the Earth's magnetic field reversed. Because the ages of these polarity reversals are known, the authors were able to qualitatively determine that the crust cooled more slowly than previously predicted from solely conductive cooling models. The temperatures of the remanence "components" are representative of a particular time interval, and so were used as an estimate of cooling rate for this lower crustal section in the doctoral dissertation of S. Maher (Maher, 2021). Our analysis above using the TROUT method corroborates the significance of these temperature estimates and additionally provides uncertainty estimates.

To explore the meaning of remagnetization temperatures, specimens from the study of Maher et al. (2021) were given two or three approximately orthogonal TRMs at temperatures close to the apparent reversal temperatures in the original thermal demagnetization experiments. If these temperatures are reproducible when thermally demagnetizing the newly acquired pTRMs, then this is evidence that the original NRM components unblock over independent temperature ranges and so can be used to obtain a quantitative cooling rate estimate. Here, we apply the TROUT method to obtain the unblocking temperature distributions, and the different CTs and MRs. Note that orthogonal magnetizations of the TRMs were not always possible, due to the specimens not being perfect cubes.

The TROUT model was fit to the 72 specimens given pTRMs by Maher et al. (2021). Some examples of fitted models are given in Figure 7 and the full set of crossover temperatures and mixed regions is shown in Figure 8. To first order, the crossover temperatures are good estimates of the original temperatures at which the pTRMs were imparted, with almost all CTs being within ±1 temperature step of the expected value and no CT being more than two steps from the expected value. The vast majority of MR ranges have a full width that spans two or fewer temperature steps, but several are wider.

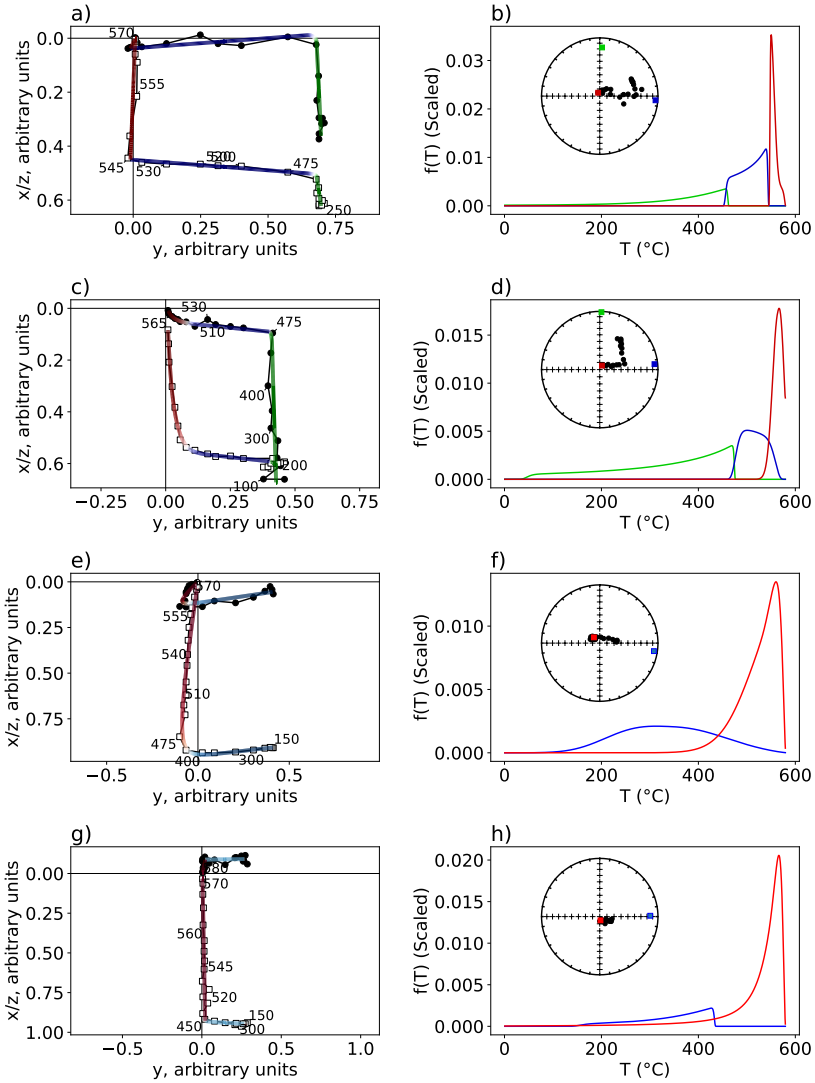

Figure 7: Results from the Pito Deep data set from specimens (top row) PD036a1, (second row) PD135a2, (third row) PD014d2 and (bottom row) PD142a2. Left column: Zijderveld plots of the data, with the model fit to the data superimposed. Colors represent the π ratio (see Section 2.4) indicating the dominant component, with red indicating the highest temperature TRM, blue indicating the moderate temperature TRM and green indicating the low temperature TRM. Center column: unblocking temperature distributions of each component. Right hand column: Equal area plots of the demagnetization data and the directions of each component. Specimen PD036a1 contains three easily resolvable components, which appear as straight lines with sharp corners on the Zijderveld plot (a) which correspond to three unblocking temperature distributions with little overlap in b). Specimens PD135a2 and PD014d2 have two or three component magnetizations with curved directions between the high and moderate (red and blue respectively) component on the Zijderveld plots (d,g), these cause overlapping unblocking temperature distributions (e,h). Specimen PD142a2 appears to have overlapping unblocking temperatures (k), despite having no curved directions on the Zijderveld plot (j). This is likely because the ratio between the two components remains fairly stable over most of the range of the low temperature component.

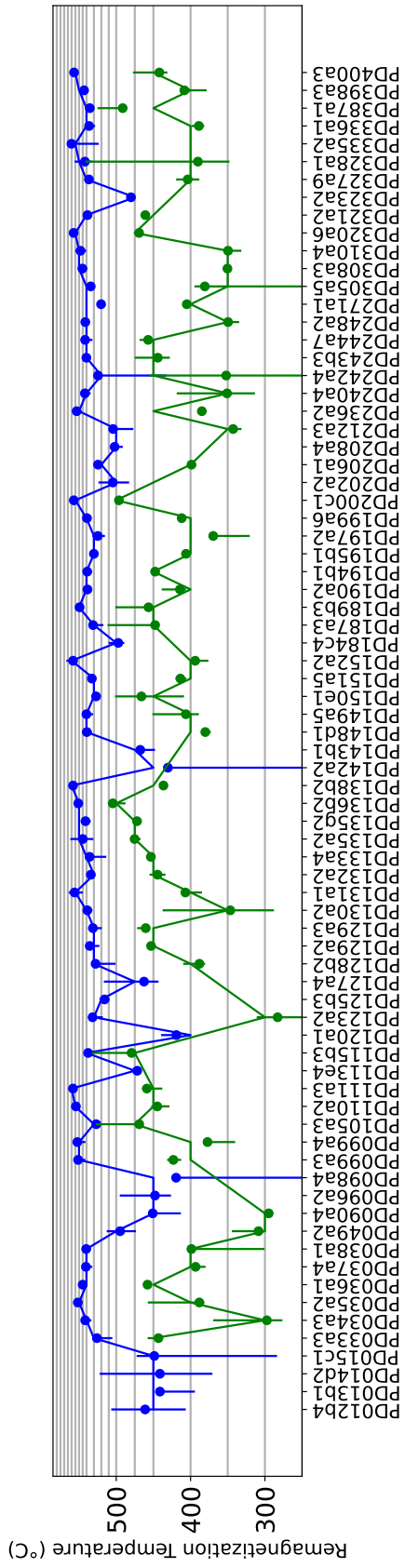

Figure 8: Estimates of the remagnetization temperatures from the Pito Deep data set using TROUT. Blue and green lines represent the temperatures at which the second and third pTRMs were applied. Blue and green dots represent the estimated crossover temperatures for the same specimens, and blue and green error bars represent the MRs for each specimen. The grey horizontal lines represent the set of temperature steps used to thermally demagnetize these specimens. In almost all cases, the crossover temperatures reproduce the original temperatures to which the TRM was heated within ±1 step. The majority of the MRs are also confined to ±1 step although there are several which are indicative of overlapping unblocking temperatures in these specimens.

In some cases, this is due to curvature observed in the directions, where there may be overlap in the unblocking temperature distributions of the two components (see Figure 7c-f). In a few cases, there appears to be overlap in the unblocking temperature distribution in regions where the directions are a straight line. This seems to occur in situations where the ratio of two unblocking temperature distributions is constant over a wide range, leading to an overestimate of the overlap (see e.g. Figure 7g,h). Although uncommon, there are a few of these cases in the Pito Deep dataset, and so the MR should be taken as an upper bound on the range of overlapping unblocking temperatures. The highly reproducible crossover temperatures and generally narrow MRs estimated for the Pito Deep data indicate that the majority of these specimens would be appropriate for use in estimating a cooling rate. Histograms of the CTs relative to the actual remagnetization temperatures, and the MR ranges are shown in Figure 9.

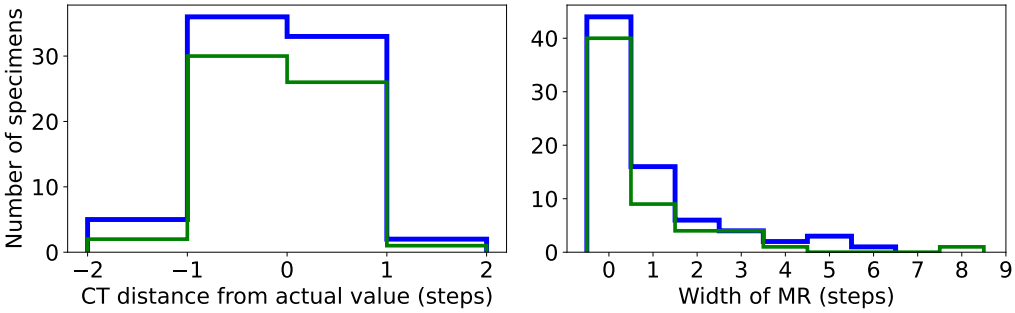

Figure 9: Plot showing histograms of a) distance of CTs from the known pTRM acquisition temperature for each specimen, measured in temperature steps, b) number of temperature steps that the MR spans for each specimen. Blue and green represent the peak temperatures of the second and third pTRM respectively. The CT is generally less than ± 1 step from the expected temperature for both components. The MR is also generally narrow (≤ 2 steps) with some exceptions. The higher temperature pTRM has a slightly wider average MR, likely due to the 5 °C temperature steps in this range.

3.2 Fragile Curvature Specimens

Santos and Tauxe (2019) characterized a set of paleomagnetic specimens which exhibited a range of behaviors in paleointensity experiments. In some specimens, the Arai plots (Nagata et al., 1963) in the original experiments were quite curved, but became straight when given a fresh TRM and subjected again to the paleointensity experiment. Then, Tauxe et al. (2021) showed that these specimens became more curved when a laboratory TRM was allowed to 'age' over a period of several years. This behavior was called 'fragile' curvature. We applied two component TRMs to specimens from the same samples, expecting that some of the specimens which produced non-ideal behavior in the paleointensity experiments would also have curved Zijderveld plots. A single TRM was applied at 600°C in one of seven directions in the laboratory x, y plane, spaced every 45°, excluding the $+x$ direction. A second pTRM was then applied at 500°C in the remaining $+x$ direction, allowing us to test effects of the angle between the two fields.

After giving specimens from Tauxe et al. (2021) two component TRMs, TROUT was used to find directions, CTs and MRs. Example results from the TROUT model are shown in Figure 10. The mean direction obtained for each pTRM orientation is plotted on an equal area projection in Figure 11a, with the high temperature directions shown in red and the low temperature direction shown in blue. The mean directions have α_{95}s

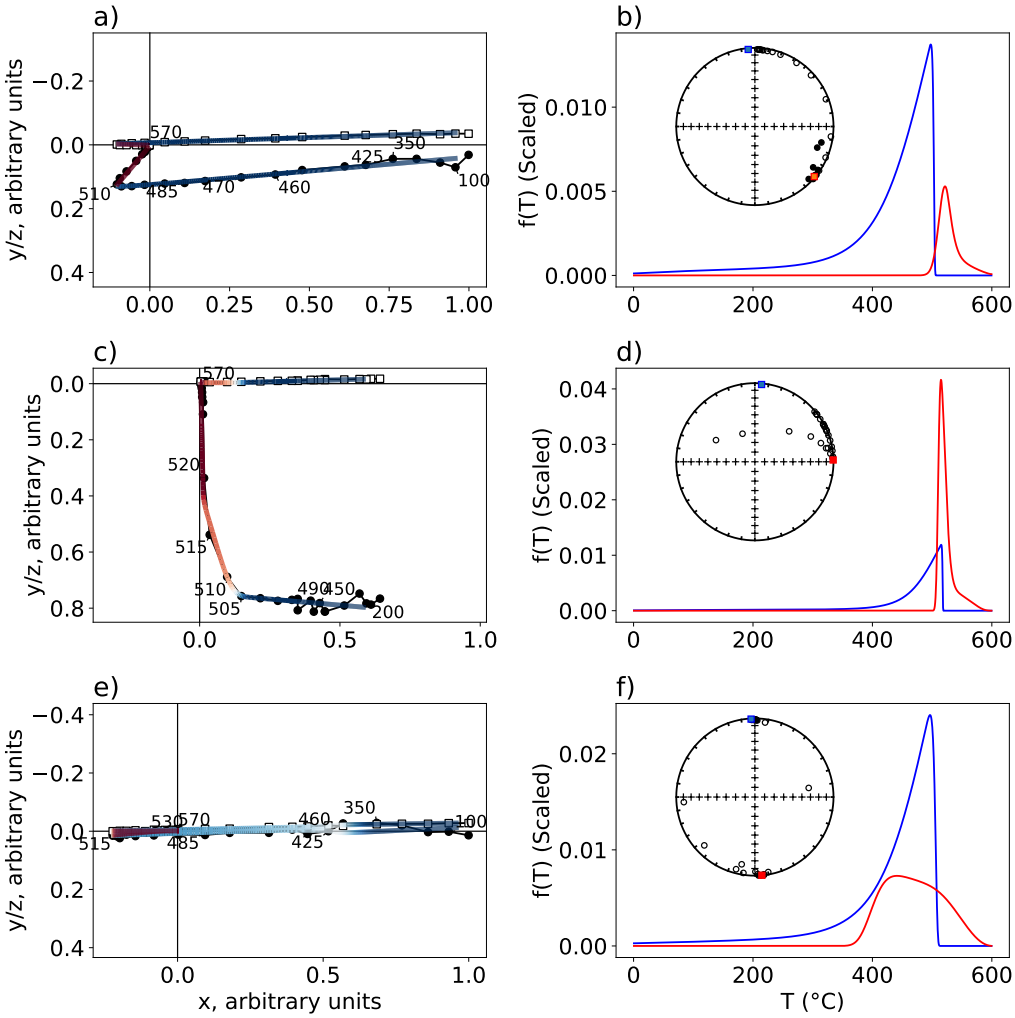

Figure 10: Examples of results from the Fragile curvature dataset from specimens (top row) mc117d, (middle row) jm009f and (bottom row) mc117e. A description of this layout is given in Figure 7. Note that specimen mc117e shows a strong overlap in the unblocking temperatures, which is due to the anti-parallel directions of the two components, which makes estimating the degree of overlap infeasible. However, the crossover temperature of this specimen is still close to 500°C.

within uncertainty of the expected direction, except for the direction with a declination of 45°. After the initial heating, the direction of the high temperature TRM was measured for each specimen. The mean measured direction of the high temperature TRMs is within uncertainty of the mean direction from TROUT for the group of 45° declination specimens, and so it is likely that the few degrees deviation of the TRMs from the expected direction is due to small misorientations of the specimens during pTRM acquisition.

Estimated CTs and MRs are shown in Figure 11b. It is noticeable that the average crossover temperature is significantly higher than the expected value of 500°C by about 5-10°C. The likely reason for this is that the specimens were given pTRMs in a sample holder constructed from a thick titanium bar which allowed them to remain up-

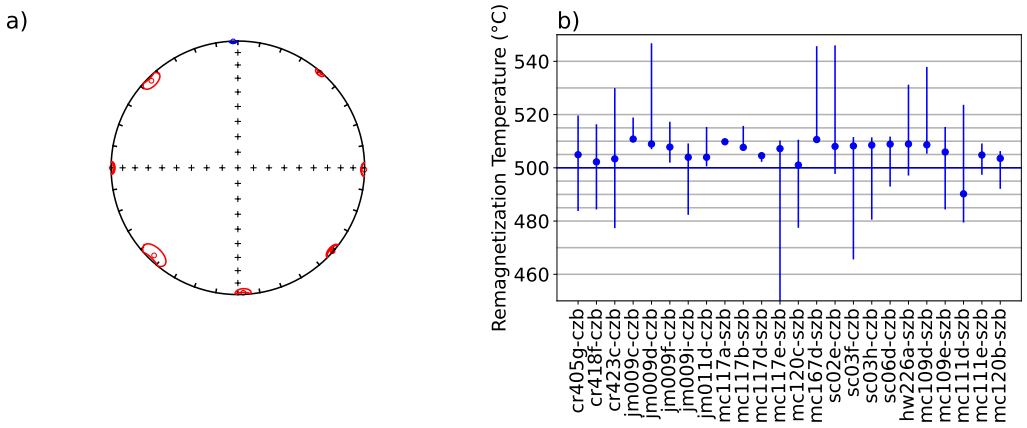

Figure 11: a) Equal area plot of mean directions obtained by TROUT for the remagnetized specimens from Tauxe et al. (2021). Blue: Low Temperature component (n = 24) and Red: High temperature directions (n = 3 or 4). Means overlap with the expected mean for each direction, except for the direction with a declination of 45°. b) Estimates of the remagnetization temperatures for the fragile curvature specimens. Blue dots are the crossover temperatures from TROUT and blue error bars are the MRs. Faint horizontal lines are the temperature steps for the thermal demagnetization experiment. specimens mc117e, mc167d, mc109e, jm009d and sc02e were magnetized in anti-parallel fields to the magnetization direction, leading to wide MRs. In general the MRs span several temperature steps, wider than the results from the Pito Deep data set (see Figure 8).

right in the paleomagnetic oven, but were demagnetized in a different sample holder in which the specimens are kept horizontally. Although the thermal gradient in the Scripps paleomagnetic oven is small, the different thermal masses of these two sample holders could explain the 5-10°C overestimate of the remagnetization temperatures observed in these specimens. No comparable temperature offset was observed for the Pito Deep samples, which were given pTRMs using a different (lower mass) sample holder.

The MRs for the specimens of Tauxe et al. (2021) are often considerably wider than those for the Pito Deep specimens, even for some of the specimens which do not exhibit curvature in their original Arai plots ("hw" and "mc" specimens). Where the two TRM directions are anti-parallel, the method generally struggles to find reasonable unblocking temperature distributions, with a wide MR often found to be favorable. However, the crossover temperature for these specimens is similar to other specimens. This makes sense, as the magnetization is effectively confined to a single dimension, overlapping unblocking temperatures will affect the magnitude but not the direction of measurements, making the unblocking temperature distributions harder to estimate. An example of this is shown with specimen mc117e in the bottom row of Figure 10. Similarly to some of the results for the Pito Deep specimens, this demonstrates that the MR may be taken as an upper bound on the range over which unblocking temperatures overlap, as it tends to be overestimated for two anti-parallel magnetizations.

3.3 MORB Reheating Experiment

Kent and Gee (1994) noted unusual behavior in a set of samples from the East Pacific Rise whereby the unblocking temperatures extended well beyond what was expected for the observed titanomagnetite Curie temperature. At the time of the study, the predominant hypothesis was that these high unblocking temperatures were carried by a new

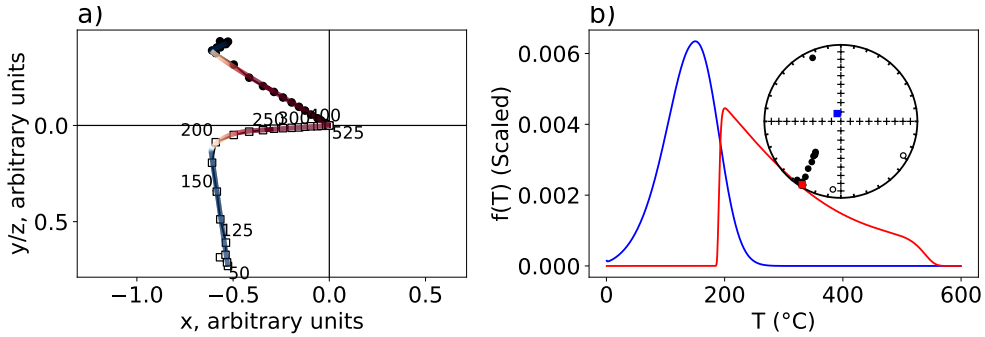

Figure 12: a) Zijderveld diagram of thermal demagnetization data of NRM plus pTRM imparted at 200°C from Figure 3 of Kent and Gee (1994). Superimposed on the original data (shown as black circles (X,Y) and open squares (X,Z) are TROUT model fits. b) Unblocking temperature distributions from the components shown in a). Inset) Equal Area plot of the directions from a) and the TROUT fit directions.

phase formed by thermochemical alteration during heating. In order to test this, Kent and Gee (1994) gave a Mid Ocean Ridge Basalt (MORB) specimen a pTRM at 200°C, the Curie temperature of TM60. Thermal demagnetization revealed a two component magnetization, with the high temperature component in the direction of the original NRM, indicating that the high unblocking temperature component could not have been newly formed during thermal demagnetization. The Kent and Gee (1994) result is shown in Figure 12. We tested TROUT on the data shown in Figure 12a as this dataset presents an excellent opportunity to explore the value of estimating CTs and MRs in a quantitative and reproducible manner. The TROUT results are plotted on top of the original data in Figure 12a. And the unblocking temperature distributions are shown in Figure 12b. The TROUT estimates are consistent with the original study.

A set of hitherto unpublished data was produced as part of the Kent and Gee (1994) investigation in which the authors imparted pTRMs in several specimens at temperatures at 50°C steps ranging from 100 to 300°C and thermally demagnetized them as in Figure 12a. We applied TROUT to that data set, estimating the CTs and MRs. The TROUT results are shown in Figure 13. The crossover temperatures are all within one step of the temperatures at which the pTRMs were imparted, and the MRs are all within ± 1-2 temperature steps. There is no evidence for any part of the pTRM component persisting to high unblocking temperatures, but the width of the MRs increases with the temperature of the pTRM. This could be caused by small amounts of thermochemical alteration, as the amount of material produced could increase with increased temperatures. This effect could also be caused by an inequality of blocking temperatures (the temperature at which the pTRM was acquired) and unblocking temperatures (the temperature at which the pTRM is demagnetized). Under this interpretation, the width of the MRs would be related to grain size. Blocking temperatures of 150°C and under have 'tight' MRs, expected for single domain grains with blocking temperatures equal to the unblocking temperature. Blocking temperatures from 200°C and above have wider MRs, which are skewed to higher temperatures, consistent with unblocking temperatures in excess of the blocking temperature, a hallmark of so-called 'high temperature' pTRM tails (Dunlop & Özdemir, 2000).

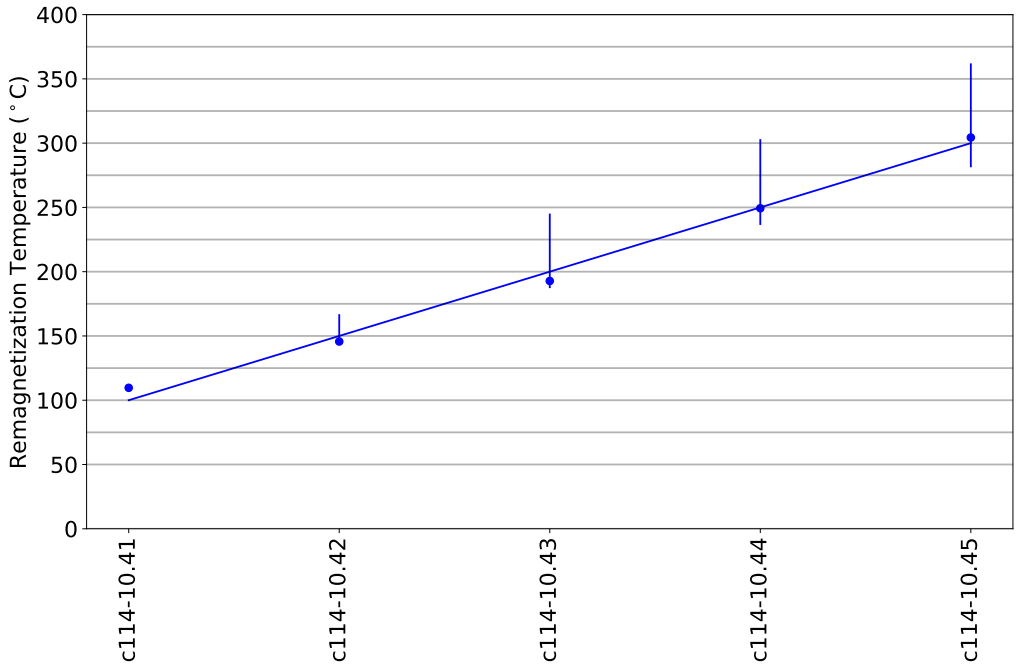

Figure 13: Estimates of the remagnetization temperatures from the MORB reheating experiment, unpublished data of Kent and Gee (1994). Blue line: pTRM remagnetization temperatures used in the MORB reheating experiment. Blue dots: crossover temperatures obtained from TROUT. Blue errorbars: mixed regions obtained from the TROUT method. Thin horizontal lines: Temperature steps used in the thermal demagnetization experiment. The crossover temperatures are all within one step, and the MRs all span 1 or 2 steps. Interestingly, the MRs widen as the pTRM temperature increases, which may be a results of high temperature pTRM tails.

4 Discussion

We have presented a method which provides a full mathematical description for a thermal or alternating field demagnetization experiment, with the ability for the unblocking temperature or coercivity spectra of components to overlap. This method can be used to obtain the direction and magnitude of each directional "component" of the magnetization, as well as information about the temperatures over which each component demagnetizes. In laboratory experiments, the TROUT method can reproduce the temperature at which a pTRM was acquired to high accuracy (usually ± 1 temperature step), even when that pTRM demagnetizes over a range of temperatures leading to a curved Zijderveld plot.

In addition to accounting for overlapping unblocking temperature ranges, the TROUT method considers both instrument noise and misorientation errors, which offers a more robust error model than principal component analysis. It can also be used to estimate the range of temperatures over which more than one magnetic component demagnetizes simultaneously, which we call the "mixed region" or MR, obtained from the overlap between the unblocking temperature distributions of each component. In general, the MR obtained from the TROUT method is controlled by the curvature of measurements on the Zijderveld plot.

There are some cases in which TROUT should not be applied. Because the model is non-unique, it sometimes returns MRs that operate over a broader range of temperatures than expected. To reduce the non-uniqueness, we utilize a prior that penalizes unblocking temperature distributions which overlap strongly. In some cases, TROUT still produces counter-intuitive MRs, particularly when two components are parallel to or antiparallel to one another (see e.g., Figure 10, bottom row) or where the two unblocking temperature distributions may completely overlap and of very different magnitudes (e.g. an IRM from a lightning strike and a TRM), where the method of intersection of planes (McFadden & McElhinny, 1988) may be more applicable. In scenarios where a component is not acquired thermally, there is generally little information to be gained from the unblocking temperature distributions. In these cases TROUT still picks accurate crossover temperatures, but will have large uncertainties in the blocking temperature distributions and magnitudes for each component.

In this paper, a "best" set of TROUT model parameters were estimated, where the posterior distribution is at a maximum. Uncertainties in these parameters can be determined by directly sampling from the posterior distribution, using a Markov Chain Monte Carlo (MCMC) method. However, results from the TROUT model have multiple posterior modes, a behavior which requires a prohibitively large number of samples for an MCMC method to accurately represent the posterior distribution. Despite this setback, MCMC sampling can be performed to form an estimate of the number of posterior modes (and therefore reasonable solutions) to the TROUT model. Examples of samples drawn from the posterior distribution using the ensemble MCMC method of Goodman and Weare (2010) for specimens presented earlier in this study are shown in Figure 14. For each of these plots, an ensemble of 64 markov chains each with 10000 samples was used to sample from the posterior, with the first 5000 samples from each chain discarded as "burn in". It is apparent that for specimens where the TROUT method yields counterintuitive results (e.g. for specimen mc117e-szb with two antiparallel components in Figure 14c-d), that there are multiple possible solutions. TROUT simply picked the solution which had a maximum posterior mode. For specimen PD014d2 in Figure 14e-f, there is also a weaker alternative mode with less strongly overlapping blocking temperatures. Alternative posterior modes can also be assessed more rapidly by looking at the range of solutions obtained by initializing the BFGS optimizer from different starting points, instead of just the best solution obtained by TROUT.

The source of overlapping unblocking temperatures in paleomagnetic specimens is likely related to the presence of magnetic grains which have different blocking and unblocking temperatures, described in Dunlop and Özdemir (2001), and which cause "fragile curvature" behavior in paleointensity experiments, as described by Tauxe et al. (2021). Micromagnetic modelling has demonstrated that certain sizes of magnetite have multiple minimum energy states which lead to unstable behavior (Nagy et al., 2017). This mechanism is consistent with the results described in Section 3.3. It could therefore be possible to use this framework to estimate the similarity between the blocking and unblocking temperatures in a paleointensity experiment. However, this is beyond the scope of this paper.

5 Conclusions

We present a mathematical model, called TROUT, which fully describes a thermal demagnetization experiment for specimens with multi-component magnetization. This model can be inverted to give us directional and thermal information about a paleomagnetic experiment. A particular advantage of the TROUT method is that it can obtain an estimate of the range of temperatures over which a remanence component demagnetizes. TROUT allows for the unblocking temperature ranges of multiple components to overlap, a behavior that has long been observed in real paleomagnetic data (e.g. Hoffman & Day, 1978). The ability for TROUT to obtain blocking temperature ranges

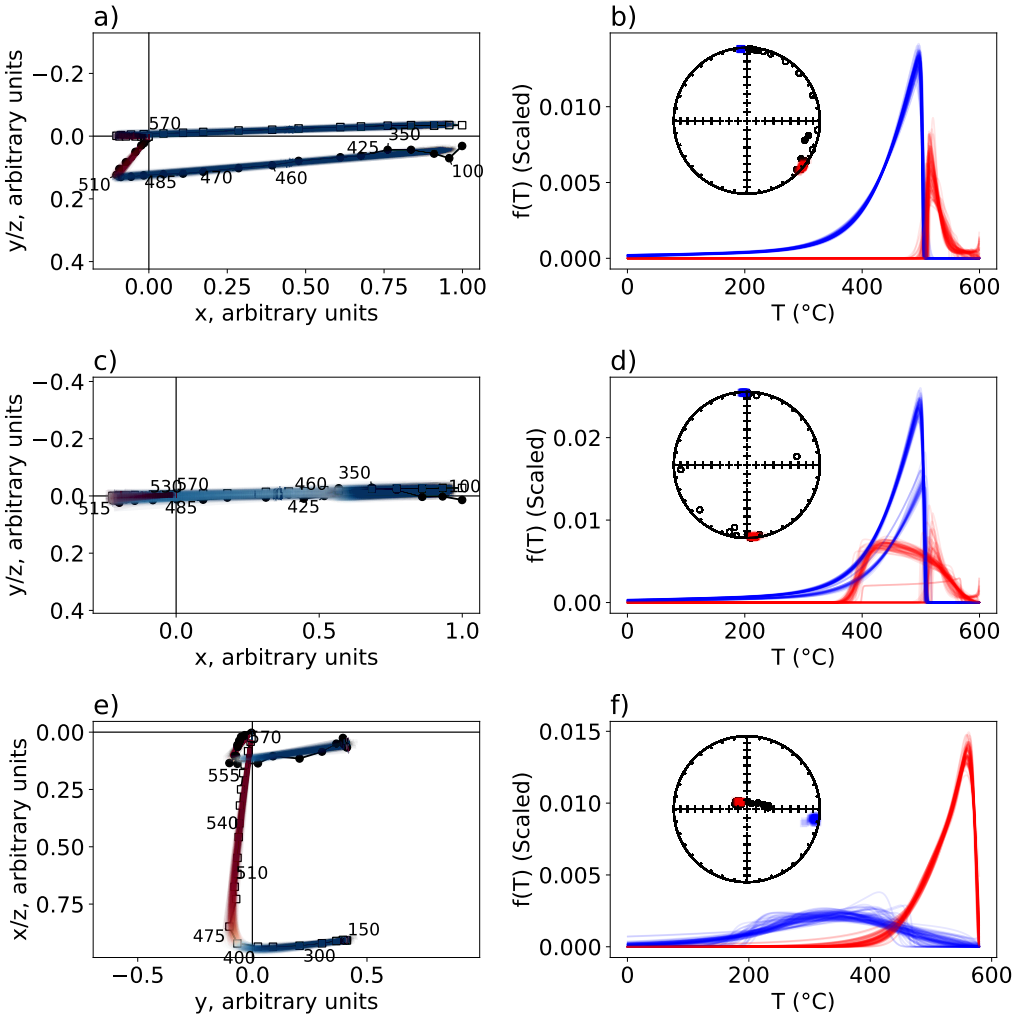

Figure 14: Samples from the TROUT posterior distribution using the Markov Chain Monte Carlo method of Goodman and Weare (2010), Zijderveld plots (left column), unblocking temperature distributions (right column) and Equal Area projections (insets) are displayed. a) and b) Samples from the posterior distribution for specimen mc117d-szb. There is little uncertainty in the unblocking temperature distribution, directions or magnitudes for this specimen. c) and d) Results for specimen mc117e-szb. The two antiparallel components in this specimen lead to uncertainties in the blocking temperature distributions and relative magnitudes (c) of the two components. However, the crossover temperature and directions of the two components have relatively low uncertainty. e) and f) Results for specimen PD014d2- there is some uncertainty in the unblocking temperature distribution of the weaker, low temperature component for this specimen, with the unblocking temperature distribution in f) showing a possible solution with less unblocking temperature overlap. Note that these samples are unlikely to sample the relative sizes of the different posterior modes equally, and so should only be used as a qualitative estimate of uncertainty.

is useful for a number of applications. Paleomagnetists wish to isolate a range of temperatures over which a single component is demagnetizing for analyzing paleodirection and paleointensity experiments, which TROUT enables. Additionally, TROUT can be

used to find the emplacement temperature of tuffs or pyroclastic flows, as well as the temperature to which a specimen was reheated, e.g. in a host rock remagnetized by an intruding dike, or an archaeological specimen where the temperature of heating is of interest. One of the advantages of TROUT is that it can be used to perform these analyses when Zijderveld plots are curved and without easily resolvable components.

We analysed three data sets containing specimens that were partially remagnetized in laboratory fields at known temperatures using TROUT. TROUT estimated the temperature at which the laboratory pTRM was acquired to within ± 1 temperature step, even for specimens where there was overlap in the unblocking temperature distributions of two components. TROUT's ability to model the unblocking temperature distributions of different components may be a useful proxy of domain state in some specimens, although care should be taken when doing this, as overlapping unblocking temperatures can be caused by effects not related to domain state, and the unblocking temperature distributions obtained by TROUT may be non-unique.

Appendix A Initialization of the optimization algorithm

In Section 2.2.3 we discussed the method used for finding the maximum of the posterior distribution. Any optimization requires initialization of the search algorithms and it was mentioned in Section 2.2.3 that an "informed guess" is computed for the set of parameters that best fit the model. Here, we describe the procedure of making an informed guess. First, the more traditional technique of obtaining directions from a thermal demagnetization experiment, using principal component analysis (PCA), is used. For a specimen with K components, the data is split into K pieces, where the minimum temperature of piece $k+1$ and the maximum temperature of piece k are shared. For each set of K pieces, the line defined by the principal component of each piece is computed. The closest point of intersection between these lines is found, and for each intersection, the lower temperature line is translated such that the two lines intersect.The end point of the lowest temperature line is set to the NRM of the specimen, and the end point of the highest temperature line is set to the magnetization of the final demagnetization step. This enables the demagnetization experiment to be described by a set of lines with connected endpoints, which is what would be expected in a Zijderveld plot with no unblocking temperature overlap.

For each of the K lines obtained from the data-splitting approach, the sum of squared distances of the measurements from the PCA lines is taken. The procedure is repeated for all possible sets of K temperature ranges, and the set of lines that minimizes the sum of squared distances is chosen. The direction of these lines is taken as an estimate of $\hat{B}$ and their lengths as an estimate of c. The lines chosen should fit the data reasonably well and will approximate the maximum posterior $\hat{B}$ and c for a specimen with no overlap between the components.

To obtain estimates of μ, s, p and q, the vector difference sum of the data in each partition is taken, divided by c and the μ, s, p^* and q^* that minimizes the squared difference between the vector difference sum and $F(x, \mu, s, p, q)$ is found using a single run of the BFGS method. By treating each component as its own demagnetization experiment, it is possible to obtain a good estimate of the μ, s, p and q that would yield a maximum a posteriori estimate if there were no overlap between components.

For σ, and ψ, values of $0.1|\vec{M}|_{\max}$ and $\pi/36$ are used as the "best guess". These parameters are intentionally set to larger values than would be expected, as initializing with a small noise tolerance may cause BFGS optimizations initialized around the guess to get trapped in local minima more frequently. Although this method of generating a best guess is complex, initializing the BFGS optimizer at a guess close to the one which

maximizes the posterior greatly increases the success rate of the optimization. This is because over a lot of the prior space, the posterior probability is effectively zero.

Acknowledgments

This work was supported in part by NSF grant EAR1827263 to LT. I would like to thank my doctoral dissertation committee, particularly Cathy Constable for her helpful feedback on this paper. We also thank Andrew Roberts for many thoughtful discussions on the uses of Bayesian techniques in paleomagnetism. All data used in this paper will be available in the MagIC database upon acceptance of the article. For the purposes of review, the data are available at: `https://earthref.org/MagIC/19659/a98614c0-1106-4b6d-a730-fd4095f84c51` and will be available at `https://earthref.org/MagIC/19659` upon publication. The code used in this paper is available at `https://github.com/bcych/TROUT`.

References

Butler, R. F. (1992). *Paleomagnetism: Magnetic Domains to Geologic Terranes.* Blackwell Scientific Publications.

Dunlop, D. J., & Özdemir, Ö. (2001). Beyond Néel's theories: thermal demagnetization of narrow-band partial thermoremanent magnetizations. *Phys. Earth Planet. Inter.*, *126*(1), 43–57. doi: 10.1016/S0031-9201(01)00243-6

Dunlop, D. J., & Özdemir, O. (2000). Effect of grain size and domain state on thermal demagnetization tails. *Geophys. Res. Lett.*, *27*, 1311-1314.

Egli, R. (2003). Analysis of the field dependence of remanent magnetization curves. *J. Geophys. Res. Solid Earth*, *108*(B2). doi: 10.1029/2002JB002023

Everitt, C. W. F., & Clegg, J. A. (1962, April). A field test of palaeomagnetic stability. *Geophys. J. Int.*, *6*(3), 312–319. doi: 10.1111/j.1365-246X.1962.tb00354.x

Goodman, J., & Weare, J. (2010). Ensemble samplers with affine invariance. *Communications in Applied Mathematics and Computational Science*, *5*(1), 65–80. doi: 10.2140/camcos.2010.5.65

Hoffman, K. A., & Day, R. (1978, August). Separation of multi-component NRM: A general method. *Earth Planet. Sci. Lett.*, *40*(3), 433–438. doi: 10.1016/0012-821X(78)90166-8

Holme, R., & Bloxham, J. (1996). The treatment of attitude errors in satellite geomagnetic data. *Phys. Earth Planet. Inter.*, *98*(3), 221–233. doi: 10.1016/S0031-9201(96)03189-5

Inman, H. F., & Bradley, E. L. (1989). The overlapping coefficient as a measure of agreement between probability distributions and point estimation of the overlap of two normal densities. *Comm. Statist. Theory Methods*, *18*(10), 3851–3874. doi: 10.1080/03610928908830127

Kent, D. V., & Gee, J. (1994). Grain size-dependent alteration and the magnetization of oceanic basalts. *Science*, *265*(5178), 1561–1563. doi: 10.1126/science.265.5178.1561

Kirschvink, J. L. (1980, September). The least-squares line and plane and the analysis of palaeomagnetic data. *Geophys. J. R. Astron. Soc.*, *62*(3), 699–718. doi: 10.1111/j.1365-246X.1980.tb02601.x

Maher, S. M. (2021). *Using magnetic methods to better understand the thermal structure of fast-spread, lower ocean crust at Pito Deep.* Retrieved from `https://escholarship.org/uc/item/01x3z748` ([Online; accessed 17. Oct. 2022])

Maher, S. M., Gee, J. S., Cheadle, M. J., & John, B. E. (2021). Three-dimensional magnetic stripes require slow cooling in fast-spread lower ocean crust. *Nature*, *597*, 511–515. doi: 10.1038/s41586-021-03831-6

McFadden, P. L., & McElhinny, M. W. (1988). The combined analysis of remagne-

tization circles and direct observations in palaeomagnetism. *Earth Planet. Sci. Lett.*, *87*(1), 161–172. doi: 10.1016/0012-821X(88)90072-6

Nagata, T., Arai, Y., & Momose, K. (1963). Secular variation of the geomagnetic total force during the last 5000 years. *J. Geophys. Res.*, *68*, 5277-5282.

Nagy, L., Williams, W., Muxworthy, A., Fabian, K., Almeida, T., Conbhuí, P., & Shcherbakov, V. (2017). Stability of equidimensional pseudo–single-domain magnetite over billion-year timescales. *Proc. Natl. Acad. Sci. U.S.A.*. ([Online; accessed 25. Aug. 2022]) doi: 10.1073/pnas.1708344114

Nagy, L., Williams, W., Tauxe, L., & Muxworthy, A. (2022). Chasing tails: Insights from micromagnetic modeling for thermomagnetic recording in non-uniform magnetic structures. *Geophysical Research Letters*, *49*, e2022GL101032. doi: https://doi.org/10.1029/2022GL101032

Néel, L. (1949). Théorie du traînage magnétique des ferromagnétiques en grains fins avec applications aux terres cuites. *Ann. géophys.*, *5*, 99–136.

Nelder, J. A., & Mead, R. (1965). A simplex method for function minimization. *Comput. J.*, *7*(4), 308–313. doi: 10.1093/comjnl/7.4.308

Nocedal, J., & Wright, S. J. (2006). *Numerical Optimization*. New York, NY, USA: Springer. Retrieved from `https://link.springer.com/book/10.1007/978-0-387-40065-5`

Paterson, G. A., Biggin, A. J., Yamamoto, Y., & Pan, Y. (2012). Towards the robust selection of Thellier-type paleointensity data: The influence of experimental noise. *Geochem. Geophys. Geosyst.*, *13*(5). doi: 10.1029/2012GC004046

Santos, C., & Tauxe, L. (2019). Investigating the accuracy, precision, and cooling rate dependence of laboratory acquired thermal remanences during paleointensity experiments. *Geochem. Geophys. Geosys.*, *20*, 383-397. doi: 10.1029/2018GC007946

Tarantola, A. (2005). *Inverse problem theory and methods for model parameter estimation*. Society for Industrial and Applied Mathematics. doi: 10.1137/1.9780898717921

Tauxe, L., Santos, C. N., Cych, B., Zhao, X., Roberts, A. P., Nagy, L., & Williams, W. (2021). Understanding nonideal paleointensity recording in igneous rocks: Insights from aging experiments on lava samples and the causes and consequences of 'fragile' curvature in arai plots. *Geochem. Geophys. Geosyst.*, *22*(1), e2020GC009423. doi: 10.1029/2020GC009423

Tauxe, L., & Staudigel, H. (2004). Strength of the geomagnetic field in the Cretaceous Normal Superchron: New data from submarine basaltic glass of the Troodos Ophiolite. *Geochem. Geophys. Geosyst.*, *5*(2), Q02H06, doi:10.1029/2003GC000635.

Williams, W., & Dunlop, D. J. (1989). Three-dimensional micromagnetic modelling of ferromagnetic domain structure. *Nature*, *337*, 634–637. doi: 10.1038/337634a0

Worm, H. U., Jackson, M., Kelso, P., & Banerjee, S. (1988). Thermal demagnetization of partial thermoremanent magnetization. *Journal of Geophysical Research-Solid Earth*, *93*, 12,196-12,204. doi: 10.1029/JB093iB10p12196

Zhao, X., Fujii, M., Suganuma, Y., Zhao, X., & Jiang, Z. (2018). Applying the Burr Type XII distribution to decompose remanent magnetization curves. *J. Geophys. Res. Solid Earth*, *123*(10), 8298–8311. doi: 10.1029/2018JB016082

Zijderveld, J. D. A. (1967). A. C. demagnetization of rocks: Analysis of results. In D. W. Collinson, K. M. Creer, & S. K. Runcorn (Eds.), *Developments in Solid Earth Geophysics* (Vol. 3, pp. 254–286). Elsevier. doi: 10.1016/B978-1-4832-2894-5.50049-5